Accuracy and Convergence of the *p*- and *hp*-Type Finite Element Methods for the Navier-Stokes Equation

Kapil K. Talwar and Bamin Khomami
Dept. of Chemical Engineering, Materials Research Laboratory, Washington University, St. Louis, MO 63130

Higher-order p and hp finite element algorithms for modeling the flow of Newtonian fluids have been developed. Numerical computations in three test geometries were carried out to compare the performance of these methods to that of conventional h-type finite elements. Computations demonstrated that for solutions which are analytic everywhere in the domain of interest, p extensions exhibit an exponential rate of convergence as opposed to the characteristic linear convergence of h-type finite element procedures. Moreover, for solutions which are analytic everywhere in the domain except at a set of points, hp extensions with geometric mesh refinement based on effective error indicators (individually, the error in the energy norm, local and global deviations from mass and momentum conservation) also give rise to an exponential convergence rate. This rapid convergence of p and hp finite element formulations enables the achievement of the solution of linear Stokes problems with an order of magnitude reduction in degrees of freedom. In nonlinear problems, these computational savings are appreciated by a factor approximately equal to the number of iterations required to obtain converged solutions.

Introduction

Finite elements and spectral methods have been used extensively in solving fluid mechanics problems in the past decade. Both methods are based on the minimization of a function corresponding to a set of partial differential equations (that is, the governing stress, continuity and constitutive equations). The conventional finite element method, here referred to as the *h* version, utilizes mesh refinement to achieve the desired accuracy, while using almost exclusively low-order polynomials of the second degree on standard quadrilateral and triangular subdomains. In contrast, global spectral techniques use higher-order polynomial degrees of approximation in a single domain to obtain solutions of a desired accuracy.

Both methods have their advantages and disadvantages. The finite element method provides substantial flexibility and is well suited for computer implementation, while the spectral method offers rapid convergence for smooth solutions. To combine the advantages of the *h* version of finite elements and spectral methods, Babuška et al. (1981) developed the *p* and *hp* versions of the finite element method. The *p* version is alluded to when fixing the mesh and increasing the polynomial degree of approximation in each subdomain. If, on the other hand, both the mesh and polynomial degrees are changed to obtain a solution of a desired accuracy, the *hp* version results.

In general, the exact solution to a problem ($\mathbf{u}_{EX}$) is often classified into three categories (Szabo and Babuška, 1990):

A. $\mathbf{u}_{EX}$ *is analytic on every finite element.* In this case, *p* extensions and global spectral techniques with their higher polynomial degrees of approximating functions provide extremely good results at a much reduced computational effort in comparison with the *h* version. The global spectral method, however, does not subdivide the flow domain, hence it is restricted to simple domains. Furthermore, the spectral discretization often results in a system of equations that tends to be ill-conditioned (Gottlieb and Orszag, 1977). To overcome this problem, finite element and difference preconditioning have been utilized successfully (Macaraeg and Streett, 1986; Canuto and Quarteroni, 1985). Moreover, Patera (1987) has recently applied the spectral method over partitioned domains. In this context, multidomain spectral methods are very similar to the *p* and *hp* version of the finite element method. Therefore, these methods would also be very effective in solving these types of problems.

Correspondence concerning this article should be addressed to B. Khomami.

B. $\mathbf{u}_{EX}$ *is analytic on each finite element except for some vertices, at which* $\mathbf{u}_{EX}$ *is a priori known to have one or more isolated singular points.* In such cases, as in problems with stress concentrations, the solution near the singularities is logarithmic in character, and polynomials are inefficient as approximating functions. Thus, both mesh refinement (extremely small elements near the singularities) and higher-order polynomials (larger elements where the solution is smooth) need to be utilized. Therefore, *hp* extensions with geometrically graded meshes, where the element size decreases in geometric progression toward the singular point (Babuška, 1988), provide excellent accuracy at minimal computational effort in comparison to the *h* version. This is due to the fact that when *hp* extensions are performed, the convergence rate of the finite element solution (as the number of degrees of freedom is progressively increased) is independent of the smoothness of the exact solution. Hence, the desired accuracy is obtained while an exponential convergence rate is maintained. Similarly, the multidomain spectral approach with optimal mesh refinement would also provide excellent solutions at reduced computational time.

C. $\mathbf{u}_{EX}$ *exhibits singular points that are solution-dependent (for example, moving boundary problems and shock phenomena).* The *hp* version with adaptive mesh refinement is currently an area of active research, and preliminary results show the extreme effectiveness of this method (Demkowicz et al., 1990).

The *p* and *hp* versions of the finite element also provide new options that the *h* version and spectral methods cannot offer. Among these is the *a posteriori* estimate of the error of the finite element solution. Babuška (1988) has shown that for linear problems, a simple relationship between the potential energy of the solution and the number of degrees of freedom in *p* extensions on a given mesh exists. This error estimate ensures the minimization of the error in the energy norm and is closely related to the root-mean-square error in stresses over the entire domain (Szabo and Babuška, 1990). These methods were originally developed for linear elastic problems in solid mechanics and are thus directly applicable to Stokes flow problems.

In this article, the accuracy and convergence rates of *p*-type finite element procedures as applied to Newtonian flow problems are discussed. The advantages of the utility of this method as compared to the conventional *h*-type finite element methods are clearly demonstrated in the following three examples. Recently, similar studies have been made in compressible and incompressible flow problems (Oden et al., 1991). This work and the investigations of Oden et al. are the only studies that utilize higher-order Galerkin methods for solving nonlinear problems.

Problem Formulation

Governing equations

The governing stress, continuity and constitutive equations for steady Navier-Stokes flow (in the absence of body forces) in two-dimensional geometries, can be expressed in the following dimensionless form:

$$Reu\cdot\nabla u=-\nabla P+\nabla^2 u \tag{1}$$

$$\nabla\cdot u=0 \tag{2}$$

where the Reynold number is given by:

$$Re=\frac{\rho\bar{u}l}{\mu} \tag{3}$$

in which ρ is the fluid density, μ is the fluid viscosity, and $\bar{u}$ is some reference velocity. The nondimensionalizations for the velocities and the isotropic pressure are performed following standard procedures (Bird et al., 1960).

Following conventional finite element procedures, we multiply the momentum equation by a trial function $w_1\hat{i}+w_2\hat{j}$, and the continuity equation by w_3, and integrate over the domain of interest. The resulting weak form of the equations is given by:

$$\int\int_\Omega\left[-P\frac{\partial w_j}{\partial x_j}+\frac{1}{Re}\tau_{ij}\frac{\partial w_j}{\partial x_i}+u_i\frac{\partial u_j}{\partial x_i}w_j\right]d\Omega = \int\int_\Omega\frac{1}{Fr}g_j w_j d\Omega+\int_\Gamma t_j w_j d\Gamma \tag{4}$$

$$\int\int_\Omega\frac{\partial u_i}{\partial x_i}w_3 d\Omega=0 \tag{5}$$

To find an approximation to $\mathbf{u}_{EX}$ (the exact solution within the domain Ω), we divide Ω into a number of three- or four-sided elements, and define a set of basis functions in Ω, so that each element has these functions defined over its space. A specific finite element mesh is defined by Δ, and the number of elements by $M(\Delta)$. The basis functions are mapped by mapping functions $Q_i[i=1,2,\ldots M(\Delta)]$ onto the elements in the global domain. The basic functions defined on Ω are characterized by the mesh Δ, the polynomial degree p, and the mapping functions. The functions are then approximated as [$N_i(\xi,\eta)$ are the basis functions]:

$$u_x(\xi,\eta)=\sum_{j=1}^{n}a_j N_j(\xi,\eta)$$

$$u_y(\xi,\eta)=\sum_{j=1}^{n}a_{n+j}N_j(\xi,\eta)$$

$$P(\xi,\eta)=\sum_{j=1}^{m}a_{2n+j}N_j(\xi,\eta) \tag{6}$$

where ξ and η form the local element coordinate system. We use the same shape functions for the trial functions w_1, w_2 and w_3:

$$w_1(\xi,\eta)=\sum_{i=1}^{n}b_i N_i(\xi,\eta)$$

$$w_2(\xi,\eta)=\sum_{i=1}^{n}b_{n+i}N_i(\xi,\eta)$$

$$w_3(\xi,\eta)=\sum_{i=1}^{m}b_{2n+i}N_i(\xi,\eta) \tag{7}$$

To ensure that a given pair of velocity and pressure trial functions yields a stable discrete scheme, the Brezzi-Babuška conditions are followed. Hence, if the discretized velocity is of polynomial degree m, then the discretized pressure cannot be of polynomial degree greater than $m-2$. Of course, in cases when the velocity is approximated by a polynomial of degree 2, the pressure can be approximated by a polynomial of degree 1.

The nodal shape functions are defined exactly as in conventional finite element methods. For higher-order polynomials, there exist side and internal shape functions (see Figure 1), which are defined in terms of a hierarchy of linear combinations of Legendre polynomials (Szabo and Babuška, 1990). Side shape functions are associated with a particular side of the standard element (quadrilateral or triangle) and are identically zero on the other sides. Internal shape functions are defined inside the element, and vanish on the periphery of the standard elements.

Boundary conditions

When an essential boundary condition is imposed at a given node (or side), the corresponding Galerkin form of the equations are replaced by the boundary conditions ($a_i=0$ and/or $a_{n+i}=0$), when these conditions are homogeneous. When they are not, we construct functions u_x^0 and u_y^0 that satisfy the boundary conditions and write the approximation as:

$$\tilde{u}_x(\xi,\eta)=u_x^0+\sum_{j=1}^{n}a_j N_j(\xi,\eta)$$

$$\tilde{u}_y(\xi,\eta)=u_y^0+\sum_{j=1}^{n}a_{n+j} N_j(\xi,\eta) \tag{8}$$

The imposed forces on the boundaries are resolved in the normal and tangential directions,

$$t_x=\sigma_{xx}\cos\alpha+\tau_{xy}\sin\alpha \tag{9}$$

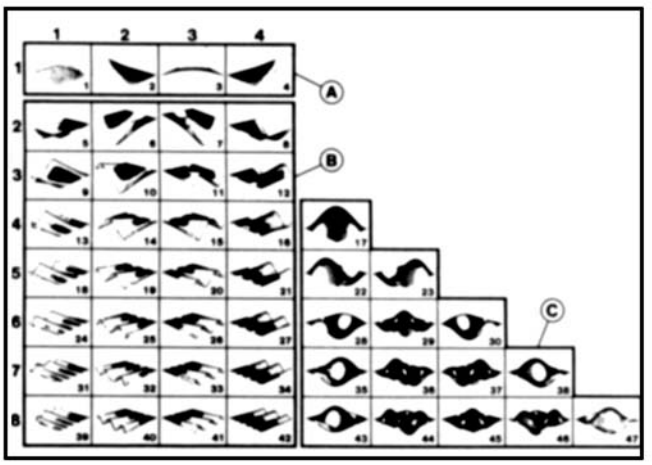

Figure 1. Hierarchic shape functions for quadrilateral elements up to $p=8$ (Szabo and Babuška, 1990).

A = vertex modes; B = side modes; C = internal modes.

$$t_y=\tau_{xy}\cos\alpha+\sigma_{yy}\sin\alpha \tag{10}$$

where α is the angle between the boundary Γ and the x-axis. Hence, the normal t_n, and the tangential, t_t, components of the imposed forces are given by:

$$t_n=t_x\cos\alpha+t_y\sin\alpha \tag{11}$$

$$t_t=t_y\cos\alpha-t_x\sin\alpha \tag{12}$$

Solution procedure

For the solution of the linear system of equations, a sparse solver was used (SMPAK), which employs a compressed storage scheme to reduce storage overhead. Solving the linearized equation involves forming the LU decomposition, where L is the lower triangular and U the upper triangular, and then obtaining successively the solution of the resulting triangular systems with the option of threshold partial pivoting during the factorization process. The solution process is essentially divided into three parts: symbolic factorization, numeric factorization, and the numeric solution, in which forward and back substitution are carried out.

When the discretized equations form a nonlinear algebraic system (such as flows with finite Reynold number), a Newton-Raphson scheme was selected to obtain the solution, with the same sparse solver being used to solve the linearized equations during each iteration. The convergence criterion used in the cases to follow was

$$\sum_{i=1}^{2n+m}\Delta a_i^2\le 10^{-4},$$

where $\Delta a_i^2=(a_i^{k+1}-a_i^k)^2$, and a_i^k represents the value of the coefficient a_i at the kth iteration. Also, the value of

$$\left|\frac{\boldsymbol{R}^{\text{old}}-\boldsymbol{R}^{\text{new}}}{\boldsymbol{R}^{\text{old}}}\right|$$

was ensured to be lower than 0.01 where $\boldsymbol{R}$ represents the residual vector.

Error estimation

Following the treatment by Szabo and Babuška (1990), we define the functionals:

$B(u,w)\equiv$ sum of terms of lefthand side of Eqs. 4 and 5 (13)

$F(w)\equiv$ sum of terms of righthand side of Eqs. 4 and 5 (14)

and the strain energy rate of the computed finite element solution is defined as:

$$U(u)=\frac{1}{2}B(u,u) \tag{15}$$

The energy norm of u in Ω is defined as:

$$\|u\|_{E(\Omega)}=\sqrt{U(u)} \tag{16}$$

where $E(\Omega)$ is the set of all functions in Ω that have finite $U(u)$. The potential energy functional is defined as:

$$\Pi(u)=\frac{1}{2}B(u,u)-F(u) \tag{17}$$

Hence,

$$\Pi(u)=U(u)-F(u) \tag{18}$$

The exact solution u_{EX} minimizes this potential energy of the system with respect to all admissible velocity/pressure functions.
That is

$$\Pi(u_{EX})=\min_{u\in E(\Omega)}\Pi(u) \tag{19}$$

[$\tilde{E}(\Omega)$ is the intersection space of $E(\Omega)$ and the set where kinematic boundary conditions are satisfied.] The finite element solution u_{FE} minimizes the potential energy with respect to all velocity/pressure functions in the space $\tilde{S}$, where $\tilde{S}=S\cap\tilde{E}(\Omega)$, and S is the discretization or the finite element space:

$$S\equiv S^{p}(\Omega,\Delta,Q)\equiv\{u\,|\,u\in E(\Omega),u_x[Q_x^{(k)}(\xi,\eta),Q_y^{(k)}(\xi,\eta)]\in S^{p_k},\\ u_y[Q_x^{(k)}(\xi,\eta),Q_y^{(k)}(\xi,\eta)]\in S^{p_k},k=1,2,\ldots M(\Delta)\} \tag{20}$$

where $x=Q_x^{(k)}(\xi,\eta)$ and $y=Q_y^{(k)}(\xi,\eta)$ are the mapping for the kth element. In other words,

$$\Pi(u_{FE})=\min_{u\in\tilde{S}}\Pi(u) \tag{21}$$

In linear problems, it has been proven that (Babuška, 1988)

$$U(u_{EX}-u_{FE})=\min_{u\in\tilde{S}}U(u_{EX}-u) \tag{22}$$

and

$$U(u_{EX}-u_{FE})\equiv\|e\|^2_{E(\Omega)}=\Pi(u_{FE})-\Pi(u_{EX}) \tag{23}$$

where $\|e\|^2_{E(\Omega)}$ is the error in the energy norm. That is to say, the finite element solution selects the functions from $\tilde{S}$ so that the error in the energy norm is minimized. Consequently, for linear problems, this is a good measure of the quality of the finite element solution. For finite Reynold number problems, this error is rendered meaningless. As will be shown, however, the behavior of other error indicators is very similar to the error in the energy norm with extensions performed on the finite element solution.

When p extensions are used in category A problems or in category B with geometric meshes, the error in the energy norm decreases approximately exponentially with the number of degrees of freedom (N), and the accuracy improves with increasing N. When the rate of convergence is approximately exponential, we write:

$$\|u_{EX}-u_{FE}\|^2_{E(\Omega)}=\Pi(u_{FE})-\Pi(u_{EX})\approx\left(\frac{k}{N^{\beta}}\right)^2 \tag{24}$$

where k and β are constants. If Π_p and N_p denote the potential energy and the number of degrees of freedom associated with a polynomial degree p, then

$$\frac{\Pi(u_{EX})-\Pi_p}{\Pi(u_{EX})-\Pi_{p-1}}\approx\left(\frac{\Pi(u_{EX})-\Pi_{p-1}}{\Pi(u_{EX})-\Pi_{p-2}}\right)^{Q}, \tag{25}$$

where

$$Q=\frac{\log\dfrac{N_{p-1}}{N_p}}{\log\dfrac{N_{p-2}}{N_{p-1}}}$$

and based on this approximation, one can get a good estimate of $\Pi(u_{EX})$.

This estimate ensures the minimization of the error in the energy norm; therefore, it is applicable to Stokes problems only. Analyzing the solution for finite Re flows entails checking the extension to which mass and momentum are conserved; this is observed in every element and over the entire flow domain as well. The expressions computed are:

$$|\text{div}|\equiv\iint|\nabla\cdot u_{FE}|\,d\Omega \text{ and } |\text{div}|_{av.}\equiv\frac{\iint|\nabla\cdot u_{FE}|\,d\Omega}{\iint d\Omega} \tag{26}$$

for each element as well as the entire domain. Note that for the exact solution, $|\text{div}(u_{EX})|=|\text{div}(u_{EX})|_{av.}=0$. These values are also compared with the value of

$$\int_{\Gamma_k}u_{FE}\cdot n\,d\Gamma$$

for each element, where n is the unit normal to the boundary of the element. In addition, we check for momentum conservation by computing the values

$$T_x^{(k)}=\int_{\Gamma_k}t_x\,d\Gamma \text{ and } T_y^{(k)}=\int_{\Gamma_k}t_y\,d\Gamma$$

over each element, where t_x and t_y are the forces acting on the element boundaries in the x and y directions, respectively. It should be realized that this is simply a measure of the inter-element stress jumps, whose existence is the consequence of applying Green's theorem in the individual macroelements.

Ideally, for a single domain in the steady flow,

$$\int_{\Gamma_k}t_x\,d\Gamma=\int_{\Gamma_k}t_y\,d\Gamma=0.$$

Hence, the resultant force $T^{(k)}=\sqrt{(T_x^{(k)})^2+(T_y^{(k)})^2}$ can be used to indicate the location of mesh refinement (the location of the maximum value of $T^{(k)}$). Note that for an ideal finite element mesh, the value of $T^{(k)}$ should be equal for every element. Consequently, the maximum value of $T^{(k)}$ in com-

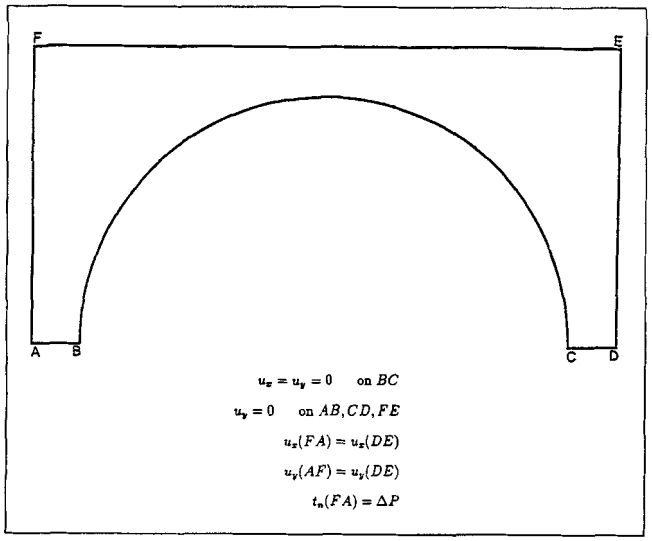

Figure 2. Domain of interest for flow past cylinders.

parison with the applied pressure drop across the domain is another indicator of the quality of the discretization.

Other than computing these equilibrium errors, we determine the value of the jumps in stresses and stress resultants across interelement boundaries, and check to see if the imposed stresses on the boundaries are recovered with sufficient accuracy.

In what follows, we have selected one problem from category A (Stokes flow past a uniform square arrangement of cylinders) and two from category B (Stokes flow in a 3:1 contraction and through an infinitely converging-diverging duct) to demonstrate the effectiveness of this method. Finite *Re* flow results are also presented for the last problem.

Test Problems

Linear problems

Transverse Flow Past a Uniform Square Arrangement of Cylinders. This problem can be reduced to the study of the flow in a unit cell with the appropriate periodic boundary conditions as shown in Figure 2. The domain *ABCDEF* represents the region through which the material flows. *BC* represents half of a cylinder of infinite length, and the boundary conditions (no slip at the cylinder surface, appropriate symmetry and periodic conditions) are indicated in the figure. Typical meshes used in our computations are shown in Figure 3. Mesh H is a representative mesh used in *h* extensions; *p* extensions are conducted on mesh P.

The computed % relative error of each extension for Stokes flow in this geometry is plotted against the number of degrees of freedom, as shown in Figure 4. The exponential convergence for *p* extensions is clearly observed, as opposed to the linear convergence of *h* extension. When the error in the energy norm falls below a predefined accepted value, say 1%, the extension process is terminated. At this point, it is important to note that there is an order of magnitude difference between the number of degrees of freedom of the two extensions. This essentially indicates the computational saving of the *p* version over the *h* version, when the error in the computed solution is the same with regard to the given norm. The next step is to

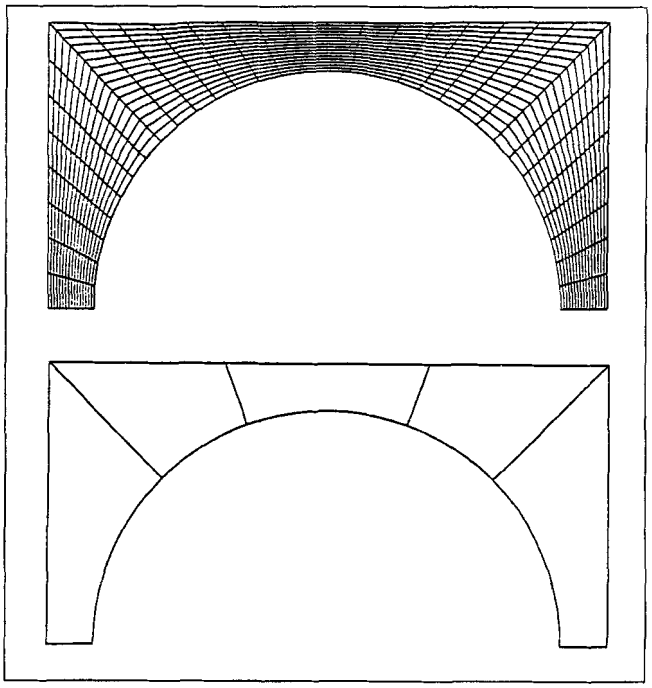

Figure 3. Finite element meshes for flow past cylinder.

Top = typical mesh for *h* extension; bottom = mesh for *p* extension.

check the quality of the finite element solution. This involves assessing the degree of interelement continuity (the residual forces by one element on the other), and verifying the conservation of mass and momentum within every element and thus over the entire domain.

Figure 5 tracks the value of $|\text{div}(u_{FE})|_{av.}$ over the entire domain. The maximum value of $T^{(k)}$ at $p=6$, at which the relative error in energy norm is 0.97%, is 3.4×10^{-3}, and its minimum value is 1.9×10^{-3}. Comparing this last value with the applied pressure drop, the largest equilibrium error is only 0.034% of the applied pressure, and the largest stress jump across the interelement boundaries is 0.032% of the applied pressure. It is interesting to note that the behavior of the $|\text{div}(u_{FE})|_{av.}$ is qualitatively similar to the error in the energy

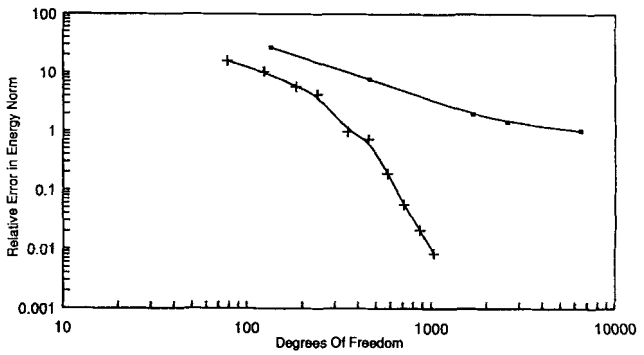

Figure 4. Computed % relative error in energy norm vs. number of degrees of freedom for flow past cylinder.

■ = *h* extension; + = *p* extension.

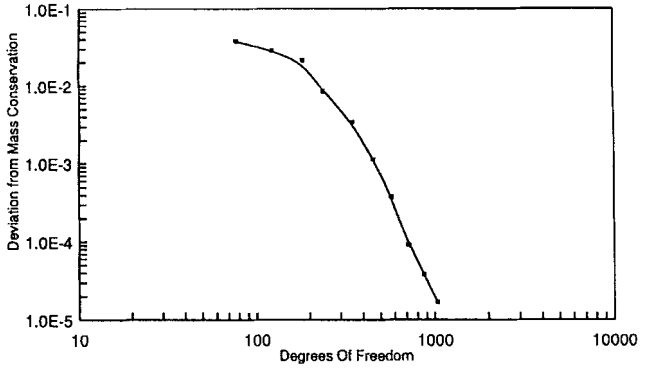

Figure 5. Computed deviations from mass conservation for entire domain vs. number of degrees of freedom.

norm. This parallelism will be seen to hold for the following two examples.

Flow through a 3:1 Contraction. Symmetry considerations reduce the domain of interest to that shown in Figure 6. The channel is chosen to be long enough to ensure fully developed flow conditions at the inlet and the outlet. The boundary *CDEF* represents the confining wall of the channel, and *AB* is the line of symmetry. *FA* and *BC* are the inlet and outlet boundaries, respectively. The pertinent boundary conditions can be seen in the figure. The spatial discretizations are shown in Figure 7, in which Mesh H is representative of refinement used during *h* extensions (note that the meshes are graded so that they are more concentrated at the dominant singularity); *p* extensions are conducted on meshes P, GP1, and GP2 (a magnified view of the section around node D is shown for mesh GP2). The latter two meshes differ in that GP2 contains two layers of mesh refinement at the singularities, whereas GP1 has only one. Meshes GP1 and GP2 are graded in geometric progression toward the corners. The innermost layer of elements are triangular, with sizes 0.15 times that of the bordering elements, a factor that has been determined to be optimum based on error analyses (Babuška, 1988).

The relative error in energy norm, for Stokes flow in this geometry, is shown for extensions on these mesh designs in Figure 8. The convergence rate of *h* extensions and *p* extensions on mesh P are approximately linear. This is due to the fact that the error in the energy norm is dominated by the effect of the singularities. In other words, the convergence rate of

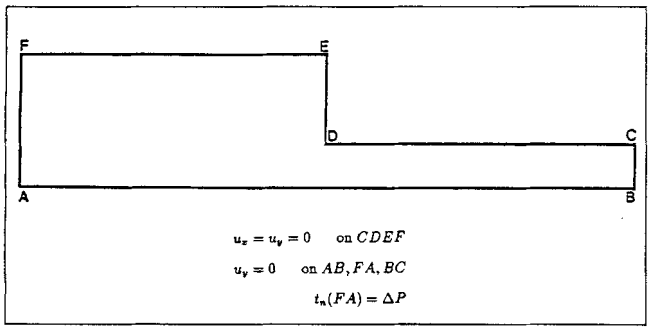

Figure 6. Computational domain of interest for flow through a 3:1 contraction.

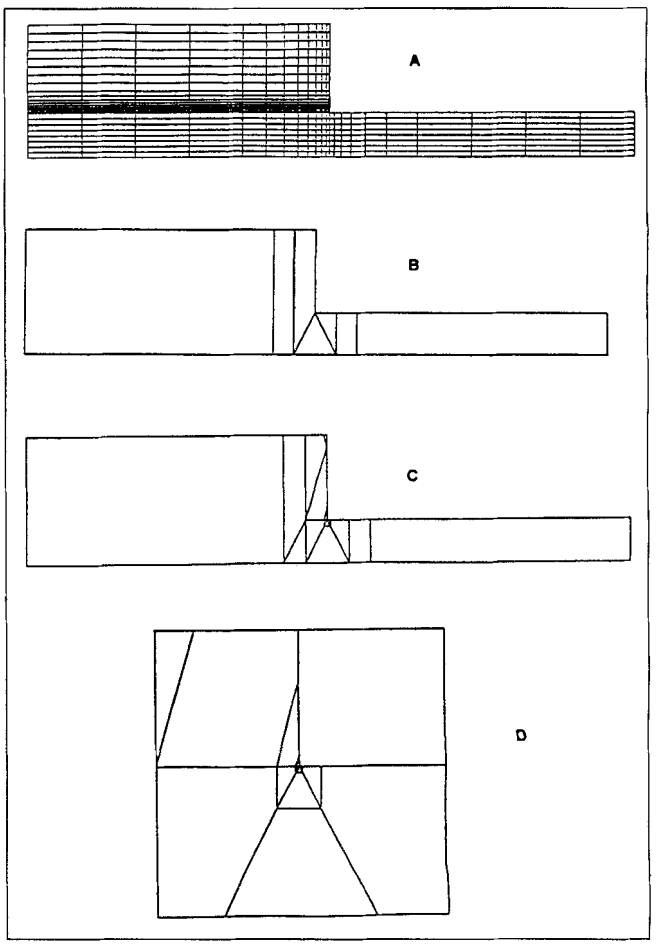

Figure 7. Finite element meshes for flow through a 3:1 contraction.

A = typical mesh for *h* extension; B = mesh P; C = mesh GP1; D = section of mesh GP2 magnified at the dominant singularity.

p-extensions is similar to that of *h*-extensions. On the other hand, *p*-extensions performed on geometrically graded meshes (GP1 and GP2) exhibit much larger convergence rates. An interesting observation is that the results of these extensions

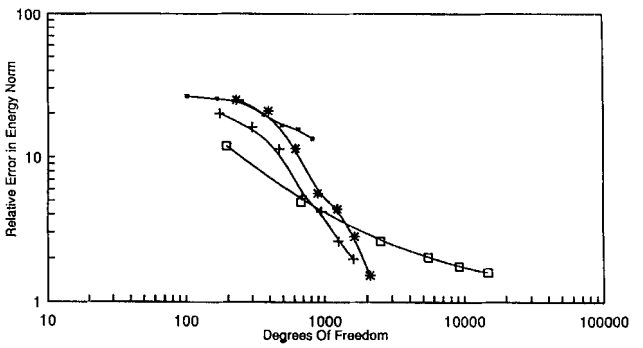

Figure 8. Computed % relative error in energy norm vs. number of degrees of freedom for flow past 3:1 contraction.

□ = *h* extension; ■ = *p* extension in mesh P; + = *p* extension on mesh GP1; * = *p* extension on mesh GP2.

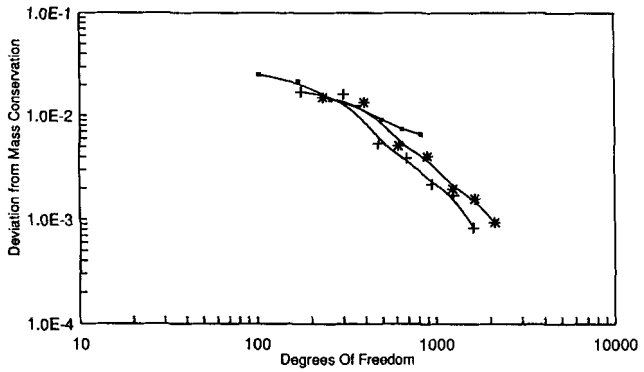

Figure 9. Computed deviations from mass conservation for entire domain vs. number of degrees of freedom for flow past 3:1 contraction.

■ = p extension over mesh P; + = p extension over mesh GP1; * = p extension over mesh GP2.

on GP2, until $p = 8$, did not show any improvement over those on GP1. This is due to the fact that the error in the energy norm at the end of the performed extensions on GP1 (when the desired accuracy was achieved) was dominated by the finite element solution in the larger subdomains, where the exact solution is known to be smooth *a priori*. Consequently, convergence is exponential, similar to the results obtained for category A problems. If the degree of polynomial were increased indefinitely, the error in the energy norm of the singly graded mesh would finally reach an asymptotic linear rate, in which the error in the solution manifests itself in the smaller elements surrounding the singularities. In other words, the final rate of convergence would be the same as that of p extensions without geometrically graded meshes. Once again, it is observed that when the error in the energy norm is around 1%, there is an order of magnitude difference between the number of degrees of freedom required by the h version, over that of the hp version, to produce a solution of similar quality (see Figure 8). This is a direct consequence of the exponential rate of convergence of hp-type methods.

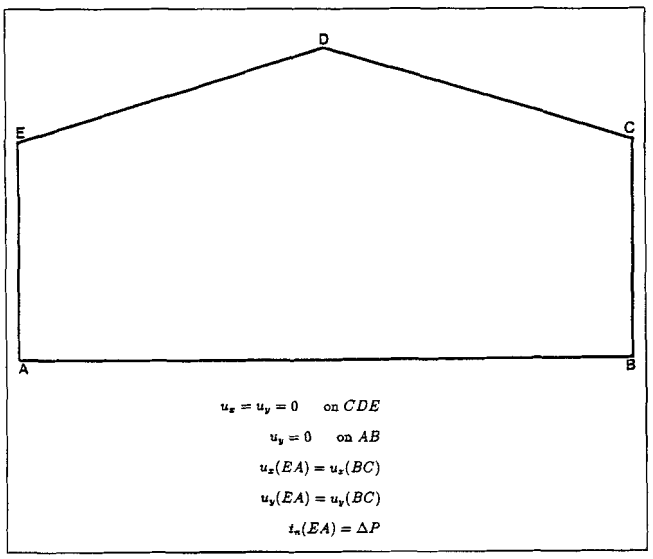

Figure 10. Computational domain for flow through an infinite converging-diverging duct.

Figure 9 is the corresponding plot of $|\mathrm{div}(u_{FE})|_{av.}$ vs. the number of degrees of freedom for p extensions on the three meshes described above. The behavior of the error in the three extensions is very similar to that in the energy norm. This presents a criterion for using similar analyses of the error in the case of nonlinear problems and utilizing the information to rediscretize the mesh adaptively. At $p = 8$, at which the error in the energy norm is 1.2%, the minimum and maximum values of $T^{(k)}$ are 4×10^{-2} and 1.63×10^{-4}, respectively. The largest equilibrium error and largest stress jump across the interelement boundaries were 0.4% and 2.4×10^{-2} of the applied pressure, respectively.

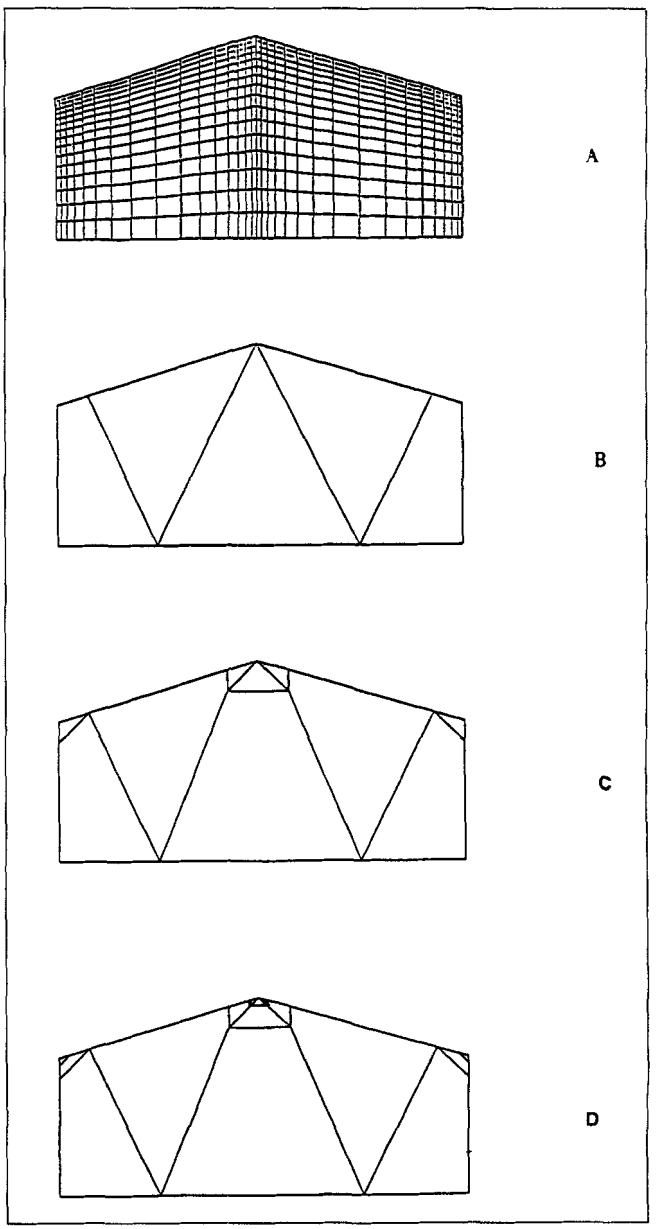

Figure 11. Finite element meshes for flow in a converging-diverging duct.

A = typical mesh for h extension; B = mesh P; C = mesh GP1; D = mesh GP2.

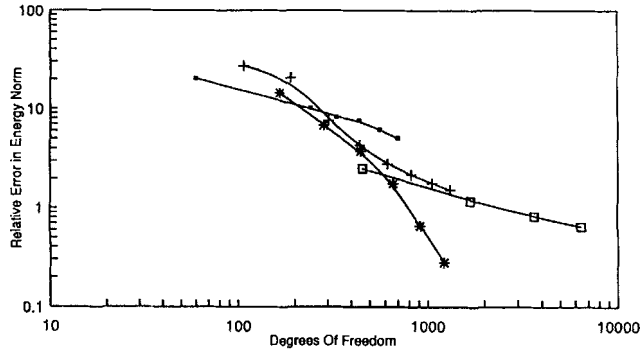

Figure 12. Computed % relative error in energy norm vs. number of degrees of freedom for flow in a converging-diverging duct.

□ = h extension; ■ = p extension over mesh P; + = p extension over mesh GP1; * = p extension over mesh GP2.

Flow through an Infinite Converging-Diverging Channel. The domain of interest can be simplified to a unit cell representative of the entire domain. This constitutes a duct that converges and diverges periodically. Symmetry considerations reduce the problem to the one shown in Figure 10. *CDE* is the solid boundary, while *AB* is the line of symmetry. Typical spatial discretizations of the flow geometry are shown in Figures 11. The respective meshes will be referenced with the same names as those in example 2.

The convergence rate of both h- and p-type finite element procedures, for Stokes flow through this geometry, are plotted in Figure 12. As expected, the h extension gives rise to a characteristic linear (algebraic) convergence rate. p extension without any mesh refinement near the geometric singular points also exhibits a linear (albeit faster) rate of convergence. A single grade of mesh refinement around the vertices (mesh GP1) increases the convergence rate only momentarily, after which it reaches its asymptotic value at $p = 5$. At this point, the error in the energy norm is unacceptably high (3%). As the figure demonstrates, increasing the p-level further would be an inefficient way to certain the error.

The convergence rate is enhanced with a second grade of mesh refinement around the vertices (mesh GP2). Exponential rates are then achieved and the computational process is terminated at $p = 7$, when the error in the energy norm is 0.28%. Once again, by using p and hp extensions with appropriate mesh refinement, we are able to achieve a solution of desired accuracy (error less than 1%) with an order of magnitude savings in degrees of freedom when compared to h extensions.

Figure 13 tracks the deviations from mass conservation for the three p extensions and for h extension. The trends appear to be similar to the error in the energy norm. The minimum and maximum values of $T^{(k)}$ are 6×10^{-2} and 5×10^{-9} (at $p = 7$), respectively. The largest equilibrium error is only 0.6% of the applied pressure drop, and the largest stress jump across the interelement boundaries is 0.4% of the applied pressure.

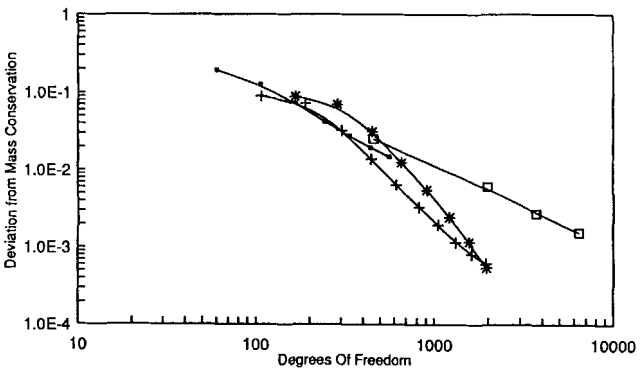

Figure 13. Computed deviations from mass conservation for entire domain vs. number of degrees of freedom for flow in a converging-diverging duct.

□ = h extension; ■ = p extension over mesh P; + = p extension over mesh GP1; * = p extension over mesh GP2.

Nonlinear problems

The three problems studied so far clearly indicate the error in energy norm to be an extremely useful tool for adaptive mesh refinement for Stokes problems, eliciting the virtues of exponential convergence of p and hp extensions. For the non-

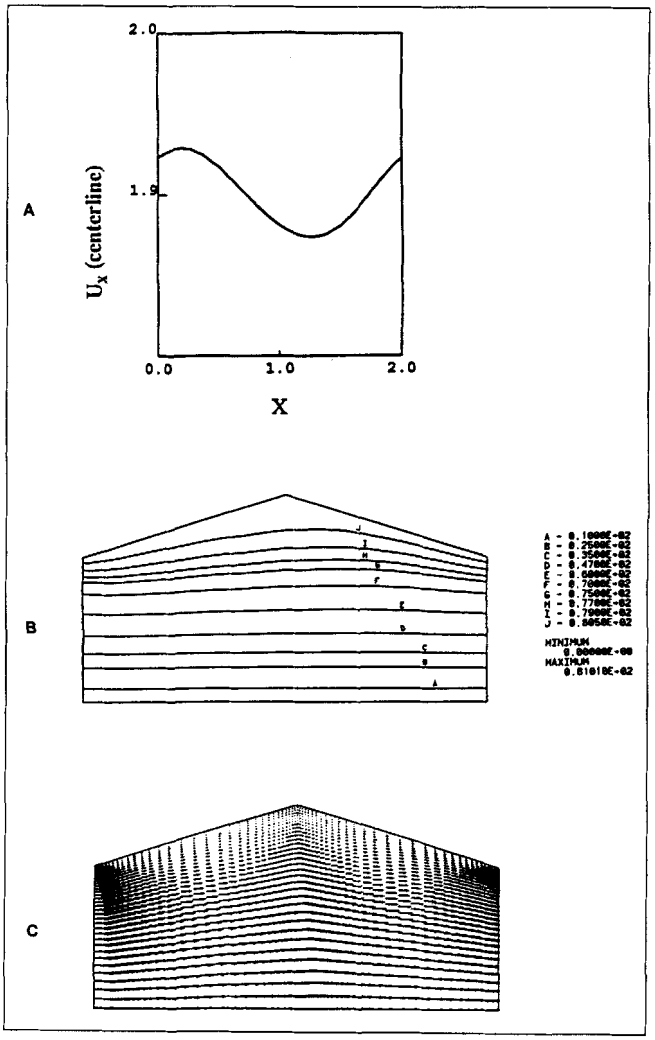

Figure 14. Representative finite element solutions at $Re = 81.01$.

A = dimensionless velocity at centerline ($u_x l/Q$, Q = flow/rate); B = streamline contours; C = velocity vectors.

linear problem, the utility of this error estimator lies in solving initially the linear problem, thus defining a minimum degree of polynomial for a given mesh. The next step is to introduce the convective terms into the problem and check the quality of the error of the new solution using the other error indicators.

To illustrate this procedure, we have selected mesh GP2 (of the last problem) primarily because it has been shown to exhibit exponential convergence for the creeping flow problem. Results for two Reynold numbers are reported, mainly $Re = 81.01$ ($\rho = \mu = 0.01$) and $Re = 156.44$ ($\rho = \mu = 0.005$). Re is identically equal to the flow rate, since the reference velocity is chosen to be the average velocity in the primary direction, and $l = 1$. The Stokes problem solution was used as an initial guess to the solution of the lower Re; the converged solution of this problem was used as an initial guess for the higher Re problem. In both cases, three Newton-Raphson iterations were necessary to satisfy the specified convergence criterion. The results of the h version were obtained in the same number of iterations with the same convergence criterion. Sample streamlines and velocity (in the primary flow direction) at the line of symmetry are shown in Figure 14.

Figures 15 and 16 plot the deviations from mass conservation against the number of degrees of freedom for these cases. An immediate observation is that the relative performance of p extension (as compared to that of h extension) has deteriorated; the exponential convergence rate of p extension is clearly lost.

To improve the performance of the scheme, the polynomial order was then allowed to vary from element to element within the domain. The underlying strategy is to achieve a solution in which every subdomain contains the same error. When there are significant variations in the interelement errors of the finite element solution, the degree of polynomial is raised in those elements within which the error is disproportionately large (this is acceptable for laminar flows, since the exact solution is known to be smooth in the regions sufficiently distant from geometric singularities). This is continued until all the elements contribute roughly the same error, after which the polynomial degree is increased in a global sense (within the entire domain). As a result of this scheme, the effort required to achieve a desired accuracy decreases sharply (the exponential convergence rate of the hp version is restored), as shown by the dashed lines in Figures 15 and 16.

The computational savings with the hp version (in comparison to the h version) are greater for nonlinear problems, since an iterative procedure is required to obtain the solution. Therefore, the computational saving is approximately equal to the number of iterations times the difference in the number of degrees of freedom required for hp and h extensions, given a desired degree of accuracy.

Conclusion

The accuracy and convergence of p- and hp-type finite element methods for low-Reynold-number, steady Newtonian fluid flow have been examined. Computation in three test geometries have demonstrated that for exact solutions, which are either analytic or piecewise analytic, adaptive p and hp extensions based on the error in the energy norm give rise to exponential convergence rates in linear Stokes problems.

In nonlinear problems, where the convective terms become important, additional error indicators such as local and global deviations from mass and momentum conservation in conjunction with the error in the energy norm have been successfully used for adaptive refinement of the meshes. As a result, exponential convergence rates in laminar flow problems have been obtained.

The rapid convergence of these higher-order methods gives rise to an order of magnitude saving in degrees of freedom for the solution of linear Stokes problems in comparison to the h version of the finite element method. For nonlinear problems that require a number of linear iterations to arrive at the solution, the computational savings are appreciated in proportion to the number of iterations required for the desired solution.

Currently, we are involved in applying these higher-order finite-element procedures to the flow of viscoelastic fluids in complex geometries to investigate their accuracy and convergence rates in flow problems containing solution-dependent singularities (very steep boundary layers).

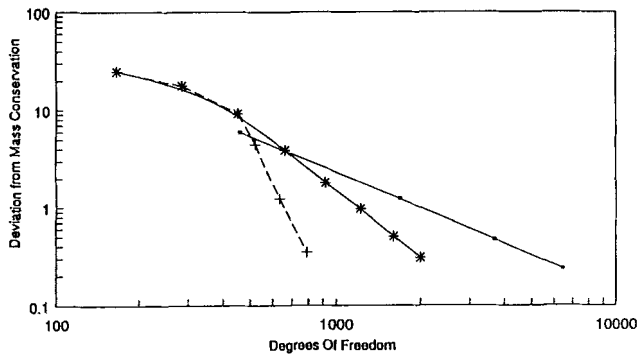

Figure 15. Computed deviations from mass conservation for entire domain vs. number of degrees of freedom for flow ($Re = 81.01$) in a converging-diverging duct.

■ = h extension; * = p extension over mesh GP2; + = hp extension over mesh GP2.

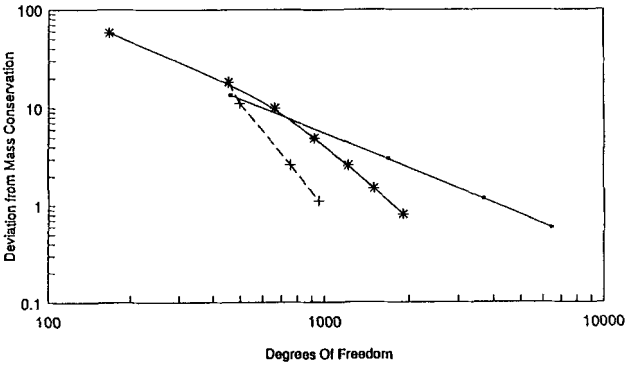

Figure 16. Computed deviations from mass conservation for entire domain vs. number of degrees of freedom for flow ($Re = 156.44$) in a converging-diverging duct.

■ = h extension; * = p extension over mesh GP2; + = hp extension over mesh GP2.

Acknowledgment

This work was supported in part by the National Science Foundation under Grant No. CTS-8914354. Computational Resources (Cray II) were provided by the University of Illinois Supercomputing Center. We are grateful to Professor B. Szabo for his valuable suggestions throughout this work.

Notation

a_j = coefficient of jth trial function
b_i = coefficient of ith test function
$E(\Omega)$ = set of all functions having finite strain energy in Ω
$M(\Delta)$ = number of subdomains
N = number of degrees of freedom
N_i = ith shape function
P = isotropic pressure
Q_i = mapping function
S = finite element space
t_j = force in jth direction
$U(u)$ = rate of strain energy
u_j = velocity in jth direction
x_i = ith axis

Greek letters

Γ_k = boundary of kth element
η = ordinate of standard element
μ = Newtonian viscosity
ξ = abscissa of standard element
Π = potential energy functional
ρ = fluid density
σ_{ij} = ijth component of total stress tensor
τ_{ij} = ijth component of extra stress tensor

Literature Cited

Babuška, I., B. A. Szabo, and I. N. Katz, "The p-Version of the Finite Element Method," *SIAM J. Numer. Anal.*, **18**, 3 (June, 1981).

Babuška, I., "The p- and hp-Versions of the Finite Element Method: the State of the Art," *Finite Elements: Theory and Applications*, D. L. Dwoyer, M. Y. Husseini, R. G. Voigt, eds., Springer-Verlag, New York (1988).

Bird, R. B., W. E. Stewart, and E. N. Lightfoot, *Transport Phenomena*, Wiley, New York (1960).

Canuto, C., and A. Quarteroni, "Preconditioned Minimal Residual Methods for Chebyshev Spectral Calculations," *J. Comp. Phy.*, **60**, 315 (1985).

Demkowicz, L., J. T. Oden, and W. Rachowicz, "A New Finite Element Method for Solving Compressible Navier-Stokes Equations Based on an Operator-Splitting Method and h-p Adaptivity," *Comp. Meth. in Appl. Mech. and Eng.*, in press (1992).

Gottlieb, D., and S. A. Orszag, "Numerical Analysis of Spectral Methods: Theory and Applications," *SIAM J. Numer. Anal.*, CBMS 26 (1977).

Macaraeg, M. G., and C. L. Streett, "Improvements in Spectral Collocation Discretization through a Multiple Domain Technique," *App. Numer. Math.*, **2**, 95 (1986).

Oden, J. T., L. Demkowicz, T. Liszka, and W. Rachowicz, "h-p Adaptive Finite Element Methods for Compressible and Incompressible Flows," *Comp. Meth. in Appl. Mech. and Eng.*, in press (1992).

Patera, A. T., "Advances and Future Directions of Research on Spectral Methods," *Computational Mechanics: Advances and Trends*, A. K. Noor, ed., AMD-Vol. 75, ASME, New York (1987).

Szabo, B., and I. Babuška, *Finite Element Analysis*, Wiley, New York (1990).

Manuscript received Dec. 18, 1990, and revision received Nov. 8, 1991.